

Investigation of low-threshold gas breakdown near solid targets by CO₂ laser radiation

A. I. Barchukov, F. V. Bunkin, V. I. Konov, and A. A. Lyubin

P. N. Lebedev Physics Institute, USSR Academy of Sciences

(Submitted October 18, 1973)

Zh. Eksp. Teor. Fiz. **66**, 965-982 (March 1974)

We investigate the formation and development of a plasma near a solid target under the influence of radiation from a pulsed CO₂ laser. The low gas-breakdown threshold of gases near targets, observed in [1], is explained theoretically. Excitation of an optically detonated wave was observed in experiment at the anomalously low excitation intensity $I \sim 10^7$ W/cm², and furthermore without preliminarily producing an absorbing plasma center by an external factor. Evaporation of solid targets by the incident radiation is studied and the gasdynamic structure of the stationary plasmotron produced thereby is analyzed. New theoretical results are obtained concerning the temperature and pressure in the region of one-dimensional vapor flow near the target. The low threshold breakdown near solids may be the cause of the damage to optical surfaces and of the limit on the maximum output power of CO₂ lasers.

1. INTRODUCTION

We have previously reported observation of breakdown of air by radiation from a pulsed CO₂ laser near solid targets; this breakdown occurs at relatively low radiation intensities $I \approx (5-10) \times 10^6$ W/cm². These experiments were continued by us recently for the purpose of investigating in greater detail the processes of formation and motion of plasma resulting from breakdown near targets. The experiments were performed in air and in argon at pressures 0.1-7 atm; the targets were a wide range of materials with different optical and thermophysical properties. The results of these experimental investigations together with their theoretical interpretation are given in Sec. 3. In Sec. 2 we discuss the possible physical mechanism of the observed low-threshold breakdown of gas near a target, a question that remained open in the first paper [1].

2. MECHANISM OF LOW-THRESHOLD GAS BREAKDOWN NEAR SOLID TARGETS

It is clear, first, that the breakdown of the initial gas (surrounding the target) is initiated under the considered experimental conditions by the onset of breakdown in vapor of the target materials near its surface. This follows from the fact that at the observed breakdown intensities $(5-10) \times 10^6$ W/cm² the condition necessary for the development of an electron cascade in the gases used in the experiment,

$$\left(\frac{\partial \epsilon}{\partial t}\right)_E = \frac{4\pi e^2 I}{mc\omega^2} \nu_{\text{eff}} > \left(\frac{\partial \epsilon}{\partial t}\right)_S^{\text{max}} = 2 \frac{m}{M} \nu_{\text{eff}} \Delta. \quad (1)$$

is not satisfied. This condition means that the rate of growth of the energy of the free electrons $(\partial \epsilon / \partial t)_E$ as a result of the inverse bremsstrahlung effect exceeds the maximum rate (in the electron energy interval $0-\Delta$) of the energy loss $(\partial \epsilon / \partial t)_S^{\text{max}}$ due to elastic collisions of the electrons with the neutral particles of the gas (e and m are the charge and mass of the electron, M is the mass of the neutral particle, Δ is the energy of its first ionization, ν_{eff} is the effective frequency of the electron collisions with the neutral particles, ω is the cyclic frequency of the radiation, and it is assumed that $\omega^2 \gg \nu_{\text{eff}}^2$). Indeed, condition (1) can be represented in the form

$$I [\text{W/cm}^2] > 6 \cdot 10^8 \Delta [\text{eV}] / \lambda^2 [\mu] A, \quad (2)$$

where A is the atomic (molecular) weight of the gas

particle. Consequently, for gas to break down by radiation from a CO₂ laser ($\lambda = 10.6 \mu$) it is necessary in any case that the radiation intensity I satisfy the condition

$$I [\text{W/cm}^2] > 5.3 \cdot 10^4 \Delta [\text{eV}] / A.$$

At the breakdown intensities observed by us, the gases (air, argon) do not satisfy this condition. At the same time, for most molecular vapors (particularly of organic compounds) the ratio is $\Delta [eV] / A \ll 1$, and accordingly condition (2) is satisfied for them at $I \sim (5-10) \times 10^6$ W/cm² and $\lambda = 10.6 \mu$.

We discuss below the following breakdown mechanism. When radiation of sufficiently high intensity I is incident on the surface of a solid target, the so-called developed-evaporation regime sets in, in which the stationary flux j of the particles of the vapor from the surface and the density N of the vapor near the surface are determined completely by the power density absorbed in the target (see, e.g., [2]):

$$j = \frac{(1-R)I}{Mq}, \quad N = \frac{j}{u} = \frac{(1-R)I}{Mqu}. \quad (3)$$

Here R is the radiation reflection coefficient, q is the specific heat of evaporation of the target material, M is the mass of the atom (molecule) of the vapor, and u is the speed of sound in the vapor at $T \sim T_{\text{cr}}$. If the diameter of the radiation spots on the surface of the target is equal to d , then the area near the surface, inside which is established the maximum vapor density N given by formula (3) has dimensions $\sim d$. The time of establishment of this region of dense vapor and the period during which it is replenished by new evaporated particles are of the order of d/u ; under the conditions of our experiments we had $d \sim 1$ mm, so that this time was $\sim 10^{-6}$ sec, i.e., short in comparison with the laser-pulse duration $\tau \approx 10-15 \mu\text{sec}$.

An electron cascade can develop in the considered region of dense vapor within a time $\sim d/u \ll \tau$. The region itself becomes strongly absorbing in this case and it is converted rapidly (within the same time interval $\sim d/u$) into a high-pressure plasma. As a result, a spherical shock wave (point explosion) is produced in the gas surrounding the target. It is precisely this shock wave which seems to make the main contribution to the momentum of the pressure on the target, which was measured in [1]. The subsequent evolution of the

breakdown plasma should depend on the radiation intensity, which continues to be incident on the front of the shock wave (see Sec. 3).

To determine how real the proposed breakdown-onset mechanism, it is necessary to estimate the values of two characteristic radiation intensities, I_{evap} —the threshold for the onset of the developed surface evaporation of the target, and I_{casc} —the threshold for the development of the cascade within a time d/u in the aforementioned region of dense vapor. The threshold intensity I_{break} of the gas breakdown due to the considered mechanism is obviously determined by the larger of the intensities I_{evap} or I_{casc} . It is precisely the intensity I_{CR} which should be compared with the experimental values in the interval $(5-10) \times 10^6 \text{ W/cm}^2$.

Our experimental data show that the investigated low-breakdown threshold was not observed at radiation intensities up to $7 \times 10^7 \text{ W/cm}^2$ for polished optical surfaces (BaF₂ and NaCl plates transparent to the CO₂ laser radiation and copper and aluminum mirrors) that were cleaned beforehand. At the same time, low-threshold breakdown took place ($I \sim 10^7 \text{ W/cm}^2$) at the same surfaces, but without prior cleaning, but the breakdown was produced only by one or two (of the earliest) pulses of the laser train. On the other hand, in the case of unpolished metallic targets, breakdown was produced in each laser pulse, and its threshold was in the interval $(5-10) \times 10^6 \text{ W/cm}^2$, the same as for nonmetallic absorbing targets (graphite, epoxy resin, etc.). These facts indicate that the investigated low-threshold breakdown is due apparently in all cases (when either metallic or nonmetallic targets are used) to evaporation of dielectric matter that absorbs strongly at the wavelength $\lambda = 10.6 \mu$. In the case of metallic targets and targets of transparent materials (BaF₂, NaCl, etc.), this matter is the impurity dielectric layer which is always present on the surface and has generally speaking a complicated multicomponent structure. On polished optical surfaces, this layer is thin and can be eliminated either by prior cleaning of the surface or by the radiation of the first laser pulse. In the case of nonmetallic absorbing targets, the evaporating matter may be either the surface impurity layer or the target material itself.

The conclusion that the observed low-threshold breakdown cannot be due to evaporation of a clean polished metallic-target surface is confirmed also by the following theoretical estimate: The threshold intensity of the developed-evaporation regime of a metallic surface is determined by the expression (see, e.g.,^[21])

$$I_{\text{evap}}^m = \frac{\rho q}{1-R} \sqrt{\frac{\chi}{t}}, \quad (4)$$

where ρ is the density of the metal, χ is its thermal diffusivity coefficient, and t is the time required to establish the developed-evaporation regime (it is assumed that $d \gg 2\sqrt{\chi t}$). It should be assumed that in our experiments $t \sim \tau/10 \sim 10^{-6} \text{ sec}$. Inasmuch as for metals $\rho q \sim 10^4 \text{ J/cm}^3$ and $\chi \sim 1 \text{ cm}^2/\text{sec}$ (for aluminum, for example, $\rho q \sim 3 \times 10^4 \text{ J/cm}^3$ and $\chi \approx 0.9 \text{ cm}^2/\text{sec}$), we obtain the estimate $I_{\text{evap}}^m \geq 10^7/(1-R) \text{ W/cm}^2$. Polished metallic surfaces (mirrors) usually have at $\lambda = 10.6 \mu$ reflectivities $R > 0.95$, so that $I_{\text{evap}}^m > 2 \times 10^8 \text{ W/cm}^2$ for such surfaces. Thus, the breakdown intensities $(5-10) \times 10^6 \text{ W/cm}^2$ realized in our experiments were indeed unable to cause evaporation of the clean metallic surfaces.

At the same time, the threshold of developed evaporation induced by radiation of wavelength $\lambda = 10.6 \mu$ lies for the overwhelming majority of nonmetallic targets precisely in the observed intensity interval (or even lower). This is the consequence of the peculiarity of radiation at wavelength $\lambda = 10.6 \mu$, namely, the absorption coefficient μ of the overwhelming majority of nonmetallic substances at this wavelength are large and amount to $\sim 10^3-10^4 \text{ cm}^{-1}$. Since the thermal conductivity of the nonmetallic substances is low and as a rule, the condition $\mu^2 \chi t \ll 1$ is satisfied, the threshold intensity of the developed-evaporation regime is determined by the formula (see, e.g.,^[21])

$$I_{\text{evap}}^{\text{nm}} = \rho q / (1-R) \mu t. \quad (5)$$

For most nonmetallic substances we have $\rho q / \mu \leq 1 \text{ J/cm}^2$, the absorptivity of the surface is $(1-R) \sim 1$, so that at $t \sim 10^{-6} \text{ sec}$ we obtain the estimate $I_{\text{evap}}^{\text{nm}} < 10^6 \text{ W/cm}^2$.

We turn now to an estimate of the intensity I_{casc} and prove first that it is determined by the single condition (2), i.e., in our case this condition is not only necessary but also sufficient for breakdown to occur. Indeed, the condition (2) becomes sufficient for cascade development if, first,

$$2 \frac{m}{M} v_{\text{eff}} \gg t_0^{-1} + t_d^{-1} \approx k \frac{u}{d} \left(1 + \frac{10}{k} \frac{u_e}{u} \frac{l_e}{d} \right) \quad (6)$$

and, second, one can neglect the energy lost by the electrons to inelastic collisions¹⁾. In (6) the quantity $t_d = \Lambda^2/D$ is the time of the free diffusion of the electron from the region of cascade development and t_0 is the lifetime of one generation of the electron cascade. In the second relation of (6) we used the fact that in our case $t_0 = d/uk$, where k is the number of necessary generations, approximately 40; $\Lambda^2 = d^2/33$ (the region of dense vapors is assumed to be cylindrical with the region of both the base diameter and the height equal to d).

The diffusion coefficient is $D = u_e l_e / 3$, where $l_e = (N \sigma_{\text{tr}})^{-1}$ is the mean free path of the electron, $u_e = \sqrt{\Delta/m}$ is the mean electron velocity, and Δ is the energy of the first ionization of the atoms (molecules) of the vapor.

Let us use formula (3) to estimate the vapor density N in the considered region of the development of the electron cascade for nonmetallic targets ($(1-R) \sim 1$); we assume $u \approx (\gamma q_1 / 10M)^{1/2}$, where $q_1 = Mq$ is the heat of evaporation per particle (γ is the constant of the Poisson adiabat). We obtain

$$N \approx 10^{13} A^{1/2} / q_1^{1/2} \quad [\text{cm}^{-3}]; \quad (7)$$

the intensity I is expressed here in W/cm^2 , and the heat of evaporation q_1 is expressed in eV. Inasmuch as for nonmetals we have $q_1 < 1 \text{ eV}$, at $I = (5-10) \times 10^6 \text{ W/cm}^2$ the vapor density is $N \geq 10^{20} \text{ W/cm}^2$. At these values of the density, the second term in the parentheses of (6) is small at $d \gtrsim 1 \text{ mm}$ in comparison with unity (the diffusion losses are inessential). The condition (6) itself ceases to depend in this case on the vapor-particle mass M and can be represented in the form

$$I \gg \frac{\gamma k}{20} \frac{q_1^2}{m u_e \sigma_1 d}. \quad (8)$$

Putting $u_e \approx 10^8$ cm/sec, $\sigma_{tr} \approx 3 \times 10^{-16}$ cm², $d \approx 1$ mm and $\gamma k/20 \approx 3$ we obtain the estimate $I \gg 3 \times 10^5 q_1^2$ (I in W/cm² and q_1 in eV). The observed breakdown intensities satisfy this estimate, and consequently the inequality (6) is satisfied under the conditions of our experiment.

As to the energy losses to inelastic collisions, under the considered conditions they can be neglected since the spontaneous emission of the excited atoms (molecules) of the vapor turn out to be "trapped" in the cascade-development region itself. This is seen from the fact that a contribution to the losses can be made only by excitations of atoms whose spontaneous-emission probability is $W > u/d$. The absorption coefficient $\mu_1 = (\lambda/2)^2 NW/\Delta\omega$ of the spontaneous emission at the wavelength λ satisfies the condition $\mu_1 > (\lambda/2)^2 Nu/\Delta\omega$ in this case. The spectral width of the absorption line is $\Delta\omega \approx Nu\sigma'$, where σ' is the effective cross section for impact broadening. Consequently, the optical thickness of the region of dense vapor, in which the electron cascades develop, relative to the possible spontaneous emission of the excited atoms, is equal to $\mu_1 d > (\lambda/2)^2/\sigma'$. Since $\lambda > 2\pi\hbar c/\Delta$, the condition for "trapping" of the spontaneous radiation $\mu_1 d \gg 1$ can be represented in the form $\Delta < \hbar c/\sqrt{\sigma'}$, which is always satisfied²⁾.

Thus, the characteristic intensity I_{casc} should be determined by condition (2), i.e., for radiation of wavelength $\lambda = 10.6 \mu$ we have $I_{casc} [W/cm^2] \approx 5.3 \times 10^7 \Delta [eV/A]$. The breakdown threshold $I_{break} = \max\{I_{evap}^{nm}, I_{casc}\}$. For substances with a ratio $\Delta[eV/A] \approx 0.1$ to 0.2, the breakdown intensity I_{break} is equal to I_{casc} ; for substances with a smaller value of this ratio, the intensity I_{break} can, to the contrary, be determined by the threshold for surface evaporation of the target and $I_{break} = I_{evap}^{nm}$. In either case, however, the quantitative estimates of I_{break} are close to the observed values $(5-10) \times 10^6$ W/cm².

In concluding this section we note that the mechanism considered above for the breakdown of gas near the target explains not only the low-threshold breakdown by CO₂ laser radiation, which was observed by us, but also the considerable lowering of the breakdown threshold observed earlier (see^[3], Sec. 5.3) in experiments with ruby ($\lambda = 0.69 \mu$) and neodymium ($\lambda = 1.06 \mu$) lasers operating in the giant-pulse regime ($\tau \sim 10^{-8}$ sec), when their emission acts on metallic and graphite targets. In these experiments, at intensities $I \sim 10^9$ to 10^{10} W/cm², a spark was produced near the target surface and was accompanied by strong absorption (screening) of the radiation. At the same time, the breakdown threshold of the surrounding air (far from the targets) was of the order of 10^{11} W/cm² for these lasers.

3. DYNAMICS OF BREAKDOWN PLASMA. EXPERIMENTAL RESULTS

The employed experimental setup is shown in Fig. 1. Radiation from a multimode pulsed CO₂ laser with transverse discharge was focused by a NaCl lens of focal length $f = 10$ cm on the surface of the target, which was placed (in some cases at an angle to the laser beam) in a chamber filled with the investigated gas. The experiments were performed in air at pressures 0.1 to 1 atm and in argon at pressures 0.1 to 7 atm. The targets were materials that were either

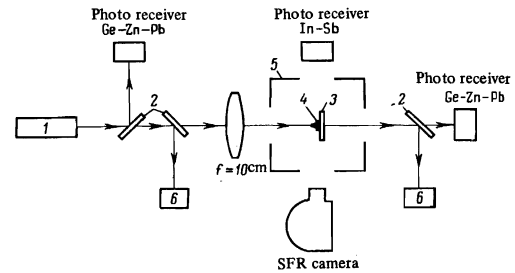


FIG. 1. Experimental setup: 1—pulsed CO₂ laser, 2—NaCl beam-splitting plates, 3—target, 4—investigated plasma, 5—chamber, 6—calorimeter.

FIG. 2. Photograph of the surface glow of a graphite target placed in the focus of a lens with $f = 1$ m.



transparent or opaque to the $\lambda = 10.6 \mu$ radiation (BaF₂, NaCl, metals, bakelite, graphite, epoxy resin).

The setup made it possible to monitor the time profile and the energy of the laser pulse, and in the case of a transparent target the same parameters were monitored for the radiation pulse that passed through the breakdown plasma. Thermocouple disk graphite calorimeters measured the energy with accuracy up to 20%. The laser-radiation receivers were Ge-Zn-Pb photoresistors; the time profile of the plasma radiation was monitored with an In-Sb photoreceiver. The signals from the receivers were fed to an SI-51 two-beam oscilloscope whose sweep was synchronized with the laser ignition.

The dynamics of the formation and the development of the breakdown plasma in the gases was investigated with an SFR high-speed motion-picture camera operating in the continuous scanning (streak) regime. The laser-pulse energy in our experiments ranged from 0.3 to 3 J, and the duration at the base was $\tau \approx 10$ to 15μ sec. The energy distribution of the beam aperture was nonuniform in character. The photograph in Fig. 2 shows the glow of the surface of a graphite sample placed at the focus of a lens with $f = 1$ m. The three spots in the distribution correspond to three parallel rows of electrons in the gas discharge of the chamber. The radiation energy for each of these spots was approximately equal, and the experimental intensities indicated later on in the article correspond to their mean values over an individual spot during the initial period of the laser pulse, with duration 4–5 μ sec. The laser beam divergence at half-power level was $\approx 10^{-2}$ rad.

If the intensity of the radiation incident on the target, I , exceeds the threshold value $I > I_{break} = \max\{I_{evap}^{nm}, I_{casc}\}$, then a bright flash of light is observed near the surface of the target and is accompanied by a characteristic "snap"—breakdown of the gas takes place. Oscillograms show that an intense glow of the plasma starts with a certain time delay relative to the start of the pulse. The characteristic delay time is $t \approx 0.5-1.5 \mu$ sec and decreases with increasing I (as a rough approximation, $t \sim 1/I$). Figure 3 shows an oscillogram of the lasing pulses and of the plasma-breakdown glow

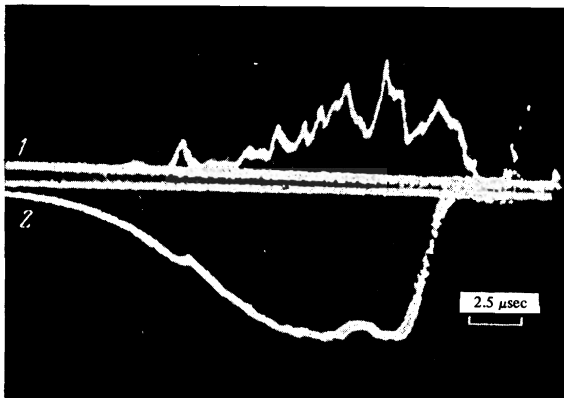


FIG. 3. Pulse oscillograms: 1—lasing, 2—plasma glow in air near a magnesium target; radiation intensity $I \approx 10^7$ W/cm².

produced in air when radiation of intensities $I \approx 10^7$ W/cm² is focused on the surface of a magnesium target.

The rest of the article will be devoted to the study of the plasma evolution that sets in after the optical breakdown (point explosion) near the target surface. The data obtained by us show that, depending on the radiation intensity I incident on the target during that period (which constitutes almost the entire duration of the laser pulse), two essentially different plasma-motion regimes are realized. When I exceeds not only I_{break} but also some other characteristic value I_{od} (see below), the breakdown plasma becomes detached from the target and the ionization front propagates with supersonic speed in a direction opposite to the laser beam (see Figs. 4a and 5a). This is the "optical detonation" regime. On the other hand, if $I < I_{\text{od}}$, then there is no detachment of the plasma from the target during the entire duration of the laser pulse. A stationary picture of three-dimensional plasma expansion into the surrounding gas, from its "hot" and dense core situated near the target surface can then set in (see Figs. 4b and 5b). We shall henceforth call this the "laser-plasmatron" regime. This dual picture of breakdown development is typical both of air and of argon in a wide range of pressures, at different experimental geometries (the lens in the front or in the rear of the target surface), and for all the investigated target materials. The only exception are polished optical surfaces, from which the optical-detonation regime is practically always realized, owing to the higher breakdown thresholds in this case.

The existence of two types of motion of a plasma produced near a target under the influence of CO₂-laser radiation was indicated also by Pirri et al.^[4], but they made no detailed study whatever of the processes of formation and development of the plasma.

We shall discuss each of these regimes separately.

A. Optical Detonation Regime

The first concepts of optical detonation were developed by Ramsden and Savic^[5] and by Raizer^[6] in order to interpret the data on the development of breakdown plasma in experiments with giant laser pulses ($\lambda = 0.69$ and 1.06μ) at radiation intensities $I \sim 10^{11}$ W/cm². In a subsequent paper^[7] Raizer has shown that to maintain the optical-detonation wave it is necessary to have radiation intensities much weaker than the gas-breakdown threshold. To initiate optical

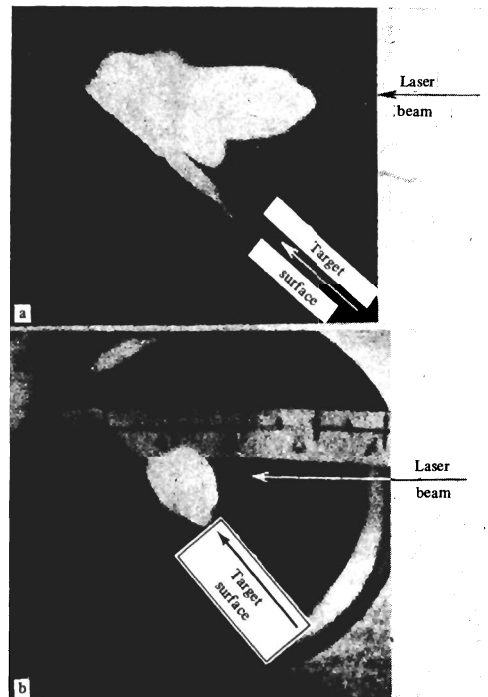


FIG. 4. Photographs of air breakdown near a brass target at $I \approx 4 \times 10^7$ W/cm² (a) and of a laser plasma in air near a magnesium target at $I \approx 1.5 \times 10^7$ W/cm². (b) The targets are placed at an angle $\approx 45^\circ$ to the laser beam, the pressure is $p_0 = 1$ atm.

detonation, according to^[7], it is necessary to produce a strongly-absorbing plasma focus, on which a light beam of intensity $I > I_{\text{od}}$ is incident. According to the estimates in^[7], in air at atmospheric pressure a light beam of wavelength $\lambda = 1.06 \mu$ and a transverse dimension $2r \approx 0.2$ cm maintains an optical detonation if the plasma-focus temperature is $T > T_{\text{min}} \approx 19\,000^\circ\text{K}$ and the intensity is $I > I_{\text{od}} \approx 8.2 \times 10^7$ W/cm². The minimum temperature T_{min} is determined in this case from the condition $\alpha(T_{\text{min}})r \approx 1$, where $\alpha(T)$ is the coefficient of absorption of the emission in the plasma, which in the case of weak ionization and at $h\nu \ll \Delta$ (Δ is the gas-particle ionization energy) can be determined from the Kramers-Unsold formula (see^[8], p. 233):

$$\alpha(T) = \frac{16\pi^2}{3\sqrt{3}} \frac{e^2 N T}{hc(h\nu)^3} e^{-\Delta/T} (e^{h\nu/T} - 1) \quad (9)$$

(N is the gas density).

In our experiments with CO₂ laser ($\lambda = 10.6 \mu$, $h\nu = 0.117$ eV), the initiating absorption focus could be the plasma resulting from low-threshold breakdown of dense vapor near the target and formation of a spherical shock wave in the surrounding gas. The transverse dimension of the laser beam in the region of the cylindrical part of the caustic amounted in our experiments to 2–3 mm, and therefore the temperature T_{min} for air, determined from the condition $\alpha(T_{\text{min}})r = 1$, turns out to be $\sim 12\,700^\circ\text{K}$. Since $I \sim T^{9/4}$ for an optical-detonation wave (see^[7]), it follows that for air at atmospheric pressure the threshold for maintaining optical detonation with CO₂ laser radiation is estimated from the formula

$$I_{\text{od}}(\lambda=10.6 \mu) = I_{\text{od}}(\lambda=1.06 \mu) (12700/19000)^{9/4} \approx 3.3 \cdot 10^7 \text{ W/cm}^2.$$

Actually, our experiments have shown that this threshold is even lower and amounts to $\approx 2 \times 10^7$ and $\approx 0.9 \times 10^7$ W/cm² for air and argon, respectively (p_0

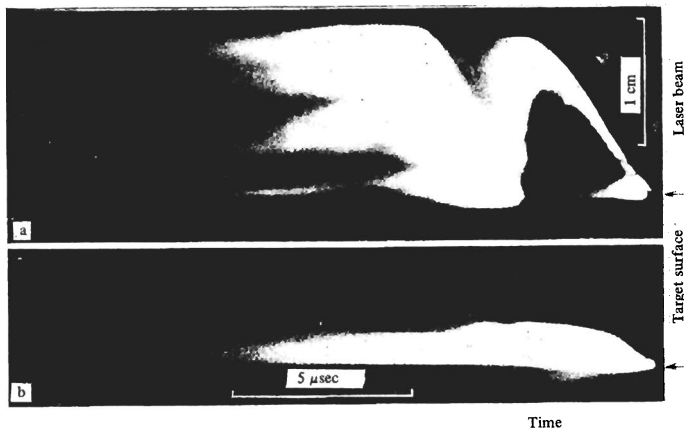


FIG. 5. Streak photographs of air breakdown near a BaF_2 target at $I \approx 4 \times 10^7 \text{ W/cm}^2$ (a) and of air near a magnesium target at $I \approx 8 \times 10^6 \text{ W/cm}^2$ (b). Pressure $p_0 = 1 \text{ atm}$.

= 1 atm). The threshold increased with increasing pressure and decreased with decreasing pressure, but there exists a certain critical pressure value below which no optical detonation is produced at all. Under our conditions, for air, this critical pressure was approximately 80 mm Hg.

Figure 5a shows a streak photograph of the breakdown of atmospheric air near a BaF_2 target at $I \approx 4 \times 10^7 \text{ W/cm}^2$. One can clearly see the plasma focus for the initiation of the optical-detonation wave, corresponding on the streak photograph to the frontal part, which fixes the motion (within the caustic) of the lens of a narrow luminous ionization front of the gas. During a certain time after its initiation, the optical-detonation wave maintains a velocity v equal approximately to $4.7 \times 10^5 \text{ cm/sec}$, and an ionization-front width equal approximately to 1.5 mm. This stage corresponds to a strong optical-detonation wave, when v is much larger than the speed of sound c_0 in the cold gas; the gas density ρ and its pressure p behind the detonation front are connected in this case with their values ρ_0 and p_0 ahead of the front by the relations (see^[9], Sec. 120)

$$\frac{\rho}{\rho_0} = \frac{\gamma+1}{\gamma}, \quad \frac{p}{p_0} = \frac{\gamma_0}{\gamma+1} \left(\frac{v}{c_0} \right)^2, \quad (10)$$

and the velocity v itself and the specific internal energy ϵ of the heated gas are given by (see^[6])

$$v = \left[\frac{2(\gamma^2-1)I\delta}{\rho_0} \right]^{1/2}, \quad \epsilon = \frac{\gamma v^2}{(\gamma^2-1)(\gamma+1)}. \quad (11)$$

Here γ is the effective adiabatic exponent of the gas behind the front of the optical detonation, γ_0 is the exponent ahead of the front, $\delta = \alpha(T)r/[1 + \alpha(T)r] < 1$ is a factor that takes into account the decrease of the "effective" intensity as a result of the loss to the lateral expansion of the gas.

Formulas (9)–(11) enable us to estimate the temperature T of the plasma of an optical-detonation wave and the absorption coefficient α in the wave. For the wave shown in Fig. 5a, putting in (10) and (11) $v = 4.7 \times 10^5 \text{ m/sec}$, $\gamma_0 = 1.4$, and $\gamma = 1.16$ (see^[8], p. 162), we obtain $\rho/\rho_0 \approx 1.85$, $p/p_0 \approx 1.2 \times 10^2$, and $\epsilon \approx 3.7 \times 10^{11} \text{ erg/g}$. Knowing the specific energy ϵ , we can, using the interpolation and thermodynamic relation $\epsilon \propto T^{3/2}$, determine the value of T . From the data of^[7] at $\epsilon = 6.7 \times 10^{11} \text{ erg/g}$ the temperature of air is $T \approx 19\,000^\circ\text{K}$. Consequently in our case we have $T = 1.9 \times 10^4 \times (3.7/6.7)^{2/3} \approx 13\,000^\circ\text{K}$. At this temperature and at a pressure $p = 120 \text{ atm}$, the absorption coefficient

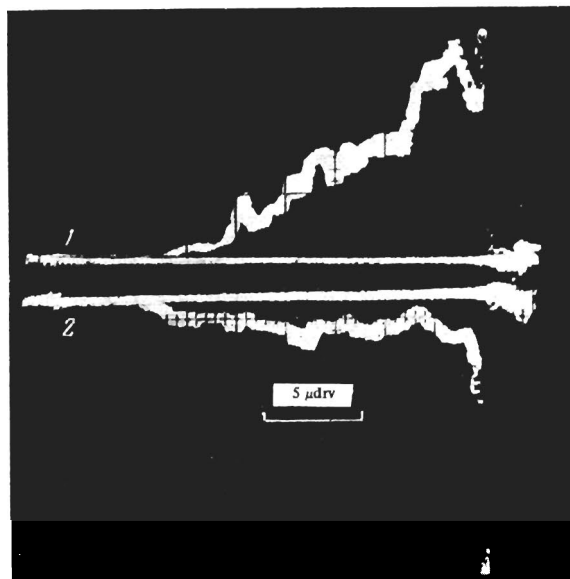


FIG. 6. Pulse oscillograms: 1—lasing, 2—radiation passing through the breakdown plasma in atmospheric air; $I \approx 4 \times 10^7 \text{ W/cm}^2$, target of BaF_2 .

of air at the wavelength $\lambda = 10.6 \mu$ is, according to (9), $\alpha \approx 12 \text{ cm}^{-1}$.

This value of the absorption coefficient is in very good agreement with the value of α determined by us in experiment. Figure 6 shows oscillograms of the incident radiation and the radiation transmitted through the breakdown plasma. The oscillograms correspond to the experiment whose streak photograph is shown in Fig. 5a; the target was a polished plate of BaF_2 , a material that is transparent to the CO_2 -laser radiation. We see that the front part of the laser pulse, preceding the development of the optical-detonation wave, passes practically without absorption. During the optical-detonation stage, the absorption increases strongly; calorimetric measurements show in this case that only $\sim 25\%$ of the incident energy of the radiation penetrates to the surface of the target.

A reduction of the oscillogram (Fig. 6) and a determination (by means of the streak photograph, Fig. 5a) of the width of the growing zone of energy released in the initial section of the optical-detonation wave (where $v \gg c_0$), make it possible to determine the value of α . Within the limits of the measurement errors, it agrees with the value $\alpha = 12 \text{ cm}^{-1}$ given above.

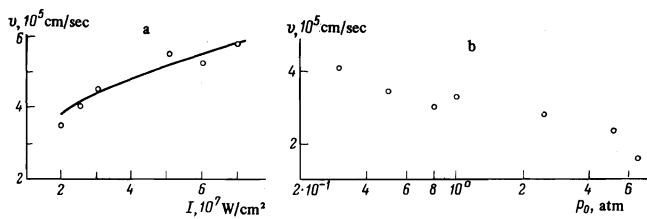


FIG. 7. Dependence of the velocity of the optical-detonation wave on the intensity of the radiation incident on a BaF_2 target in air at $p_0 = 1$ atm (a) and on the pressure p_0 of the surrounding gas (b) in argon at $I \approx 10^7$ W/cm^2 incident on a magnesium target.

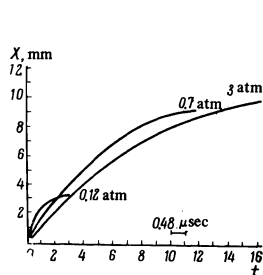


FIG. 8

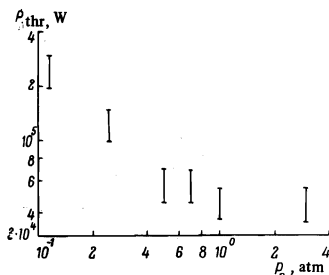


FIG. 9

FIG. 8. Time dependence of the distance to the ionization wave front. Experiments performed in argon at $I \approx 10^7$ W/cm^2 .

FIG. 9. Dependence of the slow-combustion threshold power on the argon pressure.

We have investigated experimentally also the dependence of the velocity v of the optical-detonation wave on the radiation intensity I and on the gas pressure p_0 . Figure 7a shows a plot of $v(I)$ for air; the theoretical curves corresponds to formula (11) at $\delta = 0.5$ and $\gamma = 1.16$. Figure 7b shows the dependence of v on p_0 for argon at $I \approx 10^7$ W/cm^2 . According to the theoretical concepts, in this range of pressure p_0 and intensity I , where the factor $\delta \ll 1$ (i.e., $\alpha(T, p)r \ll 1$), the velocity v should not depend on p_0 ($\delta \propto \alpha \propto p \propto p_0$ in formula (11)). With increasing value of p_0 (or intensity I), when the absorption coefficient α behind the detonation front increases and δ ceases to depend on p_0 , the velocity v , according to (11), should decrease like $p_0^{-1/3}$. The experimental data shown in Fig. 7b show that in the pressure range $p_0 \leq 1$ atm we have $\delta \ll 1$, and at $p_0 \geq 3$ atm we have $\delta \approx 0.4$ ($\alpha r \approx 0.7$). In accordance with the foregoing, the velocity v should not be dependent on p_0 in the first of these regions, whereas in the second we should have approximately $v \propto p_0^{-1/3}$. The results agree approximately with this theoretical prediction.

Let us turn again to Fig. 5a. It shows that with increasing distance from the front of the optical-detonation wave to the target the wave weakens, its velocity v decreases gradually, and the width of the front increases. Before it stops completely, at a certain definite value of the velocity, the ionization front expands jumpwise, the plasma becomes transparent, and the radiation again is incident on the target. Figure 8 shows plots of the time dependence of the distance X from the ionization front to the target surface, obtained from a reduction of the streak photographs of the plasma for different values of the gas and corresponding to the above-described initial stage of motion of the ionization front (prior to stopping).

The attenuation of the optical-detonation wave is apparently due to the decrease of the intensity of the radiation incident on its front, the decrease being caused in

turn by the increase in the area of the laser beam with increasing distance from the focus of the lens (and also by the possible decrease of the total radiation power with time). The rapid expansion of the ionization front corresponds in our opinion to a change in the gas-ionization mechanisms, namely, the optical-detonation mechanism gives way to the "slow combustion" mechanism first considered in^[10,11]. The transition from one mechanism to the other should set in at $v \equiv dX/dt = c_0$; if $v < c_0$, slow "combustion" of the gas in the laser beam takes place, the pressure jump vanishes, and the plasma becomes transparent to the radiation ($\alpha \sim 0.1$ cm^{-1}).

The stopping of the ionization front obviously corresponds to a threshold condition for the maintenance of the slow-combustion wave. According to Raizer^[11], this threshold is determined by the total power P_{thr} of the laser beam. Figure 9 shows the experimental values of P_{thr} against the air pressure p_0 , obtained from a reduction of the $X(t)$ plots shown in Fig. 8 and of the radiation-pulse oscillograms. The characteristic decrease of P_{thr} with increasing pressure p_0 , with eventual saturation, can be satisfactorily interpreted theoretically and was observed in special experiments on the slow-combustion regime (see^[12])³.

The second phase of plasma motion, represented in Fig. 5a, pertains to the laser plasmotron regime (see footnote 4 below).

B. Laser-Plasmotron Regime

If the intensity of the incident radiation I is less than the optical-detonation threshold I_{od} but exceeds the target-evaporation threshold I_{evap} , then a plasma region, a laser plasmotron, is produced near the surface of the target and exists there during the entire duration of the laser pulse. Depending on the ratio of the characteristic intensities I_{evap} and I_{casc} (see Sec. 2) and on the value of the intensity I , this plasmotron can be either stationary or pulsating. A stationary plasmotron is possible only for targets for which $I_{\text{evap}} < I_{\text{casc}}$, and the intensity of the incident radiation should lie in the interval $I_{\text{evap}} < I < I_{\text{casc}}$. On the other hand, if $I > I_{\text{casc}}$ (which should always occur for targets with $I_{\text{evap}} > I_{\text{casc}}$), then the plasmotron pulsates; the gas dynamic picture should constitute in this case a sequence of shock waves that are generated near the surface of the target and are separated by time intervals on the order of the wave-damping time (more accurately, the time after which the region occupied by the shock waves becomes so transparent that the intensity of the radiation passing through it again exceeds I_{evap}).

In our experiments at $I < I_{\text{od}}$, a plasmotron of stationary type is established for most targets (in some cases with excitation of one shock wave at the start of the laser pulse, where the power exceeds its average level; see below⁴). This fact indicates that at the wavelength $\lambda = 10.6$ μ the intensity I_{evap} for most substances turns out to be lower than I_{casc} , although, as follows from Sec. 2, the gap between I_{evap} and I_{casc} cannot be large in this case. At decreasing wavelength, this gap increases abruptly (see (2)), and in numerous experiments on evaporation of metals by millisecond laser pulses at wavelength $\lambda = 0.69$ and 1.06 μ (see^[3]), the ratio $I_{\text{casc}}/I_{\text{evap}}$ was of the order of $10^2 - 10^3$. This is precisely why the regime of stationary laser

plasmotrons was always realized in the sense indicated above. The gas-dynamic structure of this plasmotron ("plume") was first investigated in detail in^[14,15] (wavelength $\lambda = 1.06 \mu$).

We describe below the results of our experimental observation of a stationary plasmotron near the surfaces of solid targets at $\lambda = 10.6 \mu$, together with the certain new theoretical results (not contained in^[14,15]). Just as in the experiments of^[14,15], the gas dynamics of the plasmotron realized in our experiments is essentially different at low and high pressure p_0 of the external gas (air, argon).

We consider first the case of low pressures. In the steady state (the transient time is $\sim 10^{-6}$ sec) the plasma occupies two regions. The first lies near the surface of the target and has dimensions on the order of the diameter d of the irradiation spot, i.e., it coincides with the region of one-dimensional vapor flow, while the second region is located away from the first at a certain distance L along the normal to the surface; this distance depends on the gas pressure p_0 and on the intensity I of the incident radiation. The second region takes the form of a spherical segment symmetrical about the normal (see Fig. 10, a and b). In the first region, the plasma pressure p_1 greatly exceeds the external gas pressure p_0 ; this is the region of the target-vapor plasmotron heated to a definite temperature T_1 by the incident radiation. This region is the source of stationary adiabatic expansion of matter with formation of supersonic flow. The second plasma is the result of a density discontinuity (a shock wave that is immobile relative to the target), on which the super-

sonic flow of the vapor goes over into subsonic flow, the vapor pressure becomes comparable with the external pressure p_0 , and the temperature again increases to a value close to T_1 . The thickness of the segment layer in which a high plasma temperature $\sim T_1$ is preserved is determined by the rate of the plasma cooling due to recombination radiation (in our experiments this thickness amounted to several millimeters). It is clear that in the second region the plasma is not a "pure" target-vapor plasma, since the partial pressures of the vapor and of the surrounding gas become equalized in this region. We note that at sufficiently low temperatures the second ("mixed") plasma region may not arise, namely, the shock wave "goes off" to the outside of the vacuum chamber.

Figures 10a and 10b, obtained in experiments with a magnesium target placed in air at a pressure $p_0 \approx 30$ mm Hg and with incident-radiation intensity $I \sim 1 \times 10^7$ W/cm², show a bright plasmotron region near the surface of the target (first region), and a less bright second plasma region which is separated from the first by a dark gap, where the vapor expands adiabatically. It is seen from the streak photograph (Fig. 10b) that in this experiment the plasmotron regime is established without the onset of optical breakdown of the vapor, since the characteristic spark at the start of the pulse, which is observed in the optical-detonation regime (see Fig. 5a), is missing here. At the same time, we observed also cases in which the stationary-plasmotron regime was established after the occurrence of optical breakdown of the vapor; a streak photograph pertaining to this case is shown in Fig. 10c. The bright "triangle" at the start of the streak—the spark—corresponds to optical breakdown of the vapor and to propagation of a shock wave from the target (the much larger dimension of the spark in this case, in comparison with that corresponding to Fig. 5a, is due to the more than tenfold difference between the pressures p_0). It is seen from Fig. 10c that the characteristic stationary-plasmotron picture, analogous to that shown in Fig. 10b, is established after the attenuation of the shock wave (spark).

We now determine quantitatively how, first, the temperature T_1 and the pressure p_1 in the first region of the plasmotron are connected with the intensity I of the incident radiation, and, second, how the temperature T_2 in the second region is connected with the temperature T_1 , and also how the distance L between these quantities is connected with the ratio p_1/p_0 (p_0 is the pressure of the surrounding gas). We start here from the fact that the first plasmotron region, in which one-dimensional vapor flow and vapor heating by the incident radiation to a final temperature T_1 is a shock-wave region of a detonation wave with specific energy input

$$Q = \frac{(1+R)I(1-e^{-\theta})}{jM} = \frac{1+R}{1-R} q(e^{\theta}-1). \quad (12)$$

We have used for the conserved vapor flux j formula (3) in which I was replaced by $Ie^{-\theta}$, where $\theta = \int \alpha dx$ is the optical thickness of the discontinuity (of the first region).

The very need for the existence of a vapor ionization front near the evaporating target was first indicated in^[2,14].

The appearance of the detonation discontinuity is due to the fact that the supersonic flow of the "cold" (and

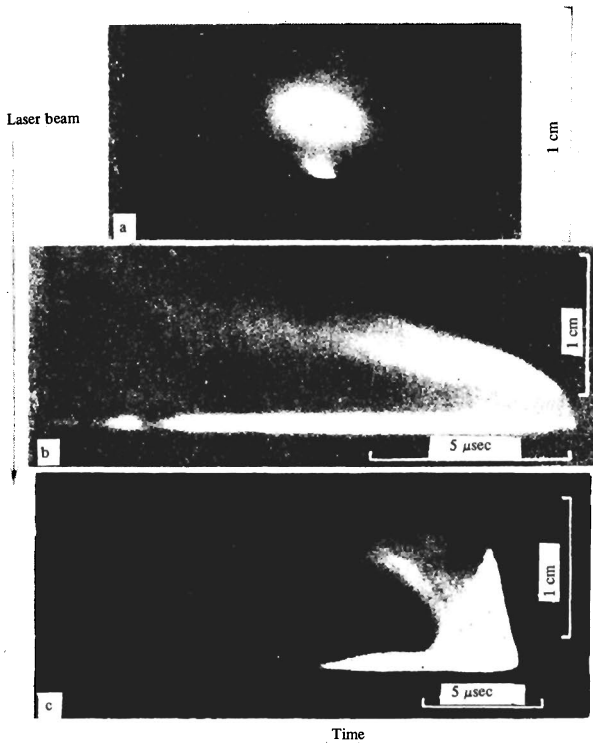


FIG. 10. a) Photograph of laser plasma in air at $p_0 \approx 30$ mm Hg near a magnesium target, $I \approx 10^7$ W/cm²; b) streak photograph of the motion of the laser plasma under the same conditions; c) streak photograph of the motion of the laser plasma in air at $p_0 \approx 60$ mm near a magnesium target, $I \approx 1.5 \times 10^7$ W/cm².

therefore transparent) vapor in the rarefaction wave propagating from the target in a direction opposite to the incident radiation is unstable. The second type of hydrodynamic flow possible here, which is stable, is precisely a detonation wave with maximum possible per unit energy input Q (i.e., with maximum optical thickness θ). Since the detonation front is immobile relative to the target, the maximum energy input Q corresponds to the maximum vapor velocity in the rarefaction wave u_{\max} , i.e.,

$$[2(\gamma_1^2 - 1)Q]^{1/2} = u_{\max}. \quad (13)$$

The left-hand side of this equation determines the velocity of the strong detonation wave; γ_1 is the adiabatic constant behind the detonation front (see^[9], Sec. 120). The maximum vapor velocity u_{\max} can be connected with the vapor temperature T_0 on the surface of the weak discontinuity from which the rarefaction wave propagates, i.e., essentially with the temperature corresponding to the start of the hydrodynamic flow of the vapor from the target (behind the Knudsen layer) (see^[3], Sec. 4.1):

$$u_{\max} = c_0 \frac{\gamma_0 + 1}{\gamma_0 - 1} = \left(\gamma_0 \frac{T_0}{M} \right)^{1/2} \frac{\gamma_0 + 1}{\gamma_0 - 1}, \quad (14)$$

where γ_0 is the adiabatic constant ahead of the detonation front and M is the mass of the vapor particles. The temperature T_0 is in turn always close to the temperature T of the target surface. For targets with unity vapor-particle "trapping" coefficient β , (for example, metals), a kinetic calculation yields (see^[3], Sec. 4.1) $T > T_0 > 0.65T$.

Formulas (12)–(14) lead to the following expression for the optical thickness of the first plasmotron region:

$$\theta = \ln \left[1 + \frac{\gamma_0}{2(\gamma_1 - 1)} \left(\frac{\gamma_0 + 1}{\gamma_0 - 1} \right)^2 \frac{1 - R}{1 + R} \frac{T_0}{q_1} \right], \quad (15)$$

where $q_1 = qM$. Hence, using the known expression for the temperature T_1 behind the front of the strong detonation wave (see^[9], Sec. 120), we obtain

$$T_1 = \frac{2\gamma_1}{\gamma_1 + 1} \frac{Q}{C_{v1}} = \frac{\gamma_0 \gamma_1}{(\gamma_1 + 1)^2} \left(\frac{\gamma_0 + 1}{\gamma_0 - 1} \right)^2 T_0. \quad (16)$$

To determine the pressure p_1 it is necessary to use the momentum-flux conservation law in the region of the one dimensional flow of the vapor, and the Chapman-Jouguet condition, namely, the vapor flow velocity v_1 behind the detonation front must be equal to the local velocity of sound c_1 . This yields $p_1 = p/(1 + \gamma_1)$, where p is the vapor pressure on the very surface of the evaporating target. At a given surface temperature T , the pressure p is always close to half the saturated-vapor pressure $p_S(T)$; for targets with $\beta = 1$, for example, calculation yields $p = 0.56 p_S(T)$ (see^[3], Sec. 4.1). On the other hand, the pressure $p_S(T)$ is connected with the vapor flux j , and consequently, according to (3), also with the radiation intensity I . The flux j is always close to the flux of evaporation into vacuum $j_{\text{vac}} = p_S(T)/\sqrt{2\pi MT}$; at $\beta = 1$ we have $j = 0.82j_{\text{vac}}$ (see^[3], Sec. 4.1). Assuming for the sake of argument the presented numerical values of the coefficient (at $\beta = 1$) and using (3), we obtain

$$p_1 = 1.7 \frac{(1 - R) I e^{-\theta}}{(1 + \gamma_1) q} \sqrt{\frac{T}{M}} \quad (17)$$

(when using (3) we have again replaced I by $I e^{-\theta}$).

Formulas (15)–(17) yield a solution of the first problem, namely, they connect T_1 and p_1 with the intensity I of the radiation incident on the target. The target-

surface temperature in the developed-evaporation regime (the only one we are considering at present) depends on I only logarithmically; according to Eq. (13) of^[2] and formula (15), we have

$$T = q_1 \ln \left\{ \frac{I_\infty}{I} \left(\ln \frac{I_\infty}{I} \right)^{1/2} \left[1 + \frac{\gamma_0}{2(\gamma_1^2 - 1)} \left(\frac{\gamma_0 + 1}{\gamma_0 - 1} \right)^2 \frac{1 - R}{1 + R} \frac{T_0}{T} \ln^{-1} \frac{I_\infty}{I} \right] \right\} \\ I_\infty = \frac{p^{(0)} q_1^{1/2} \exp(q_1/T_{\text{boil}})}{(1 - R) \sqrt{2\pi M}} \quad (18)$$

where T_{boil} is the normal boiling temperature of the target material and $p^{(0)} = 1$ atm. Typical values of the characteristic intensity are $I_\infty \sim 3 \times (10^8 - 10^9)$ W/cm². At incident-radiation intensities $I \sim 3 \times 10^6$ to 10^7 W/cm², the typical values of the temperature T lie in the interval $q_1/10 \lesssim T \lesssim q_1/5$, i.e., the temperature T is always close to the critical temperature T_{CR} of the target material^[5].

Thus, according to (15), (16), and (18), the temperature in the first region of the stationary plasmotron and its optical thickness θ depend only logarithmically on the intensity I of the incident radiation, and the pressure p_1 in it is proportional with high accuracy to I .

To establish a connection between T_1 and T_2 , and also between L and p_1/p_0 , it is necessary, first, to use the fact that with increasing distance from the first region of the plasmotron, along the normal to the surface, in the region of the three-dimensional adiabatic expansion of the vapor, the Bernoulli equation and the Poisson adiabat equation should hold true, and the conservation law for the flow of the material should take the form

$$\rho' v' = \rho_1 v_1 \sin^2 \theta, \quad (19)$$

where ρ_1 and $v_1 = c_1$ are the vapor density and its velocity on leaving the first region (i.e., behind the detonation front), ρ' and v' are the values of these quantities at that point normal to the surface from which the radiation spot is seen on it at an angle 2θ . This point can lie, in particular, also on the front of the shock wave, i.e., on the boundary of the second region of the plasmotron; the pressure p' and the temperature T' ahead of the shock are then connected with the pressure $p_2 = p_0$ and the temperature T_2 in the second region of the plasmotron by the customary shockwave relations (see^[9], Sec. 85). The resultant system of equations makes it possible to express all the hydrodynamic quantities pertaining to the second plasmotron region, and also the distance between the regions

$$L = 1/2 d (\sin^2 \theta - 1)^{1/2},$$

in terms of the quantities T_1 , p_1 , ρ_1 , and v_1 (d is the diameter of the irradiated spot). The solution of this problem assumes the simplest form at $L \gg d$. The temperatures are then connected by the relation

$$T_2/T_1 = 2\gamma/(\gamma + 1), \quad (20)$$

and the distance is

$$L = d \left[\frac{\gamma}{2(\gamma^2 - 1)^{1/2}} \frac{p_1}{p_0} \right]^{1/2}. \quad (21)$$

On the basis of (21), the condition for the applicability of formulas (20) and (21) ($L \gg d$) can be written in the form

$$p_0 \ll \frac{\gamma}{20(\gamma^2 - 1)^{1/2}} p_1. \quad (22)$$

This condition is essentially the criterion for the small-

ness of the pressure p_0 at which, under stationary conditions, supersonic expansion of the vapor is observed, and at the same time the two regions of the plasmotron should exist. For typical experimental conditions ($I \approx 10^7$ W/cm², $\theta \approx 1$, $R \approx 0.5$, $q \approx 5 \times 10^3$ J/g, and $\sqrt{T/M} \approx 10^5$ cm/sec), taking (17) into account, we obtain the estimate $p_0 \ll 1$ atm.

It follows from formula (20) that temperatures in both plasmotron regions, even when condition (22) is satisfied (when $L \gg d$), are always close to each other. Formulas (21) and (17) show that in the region of the pressures p_0 satisfying the condition (22) we have $L \propto (I/p_0)^{1/2}$. The relation $L \propto p_0^{1/2}$ was first theoretically predicted and experimentally confirmed^[14]. As to the relation $L \propto I^{1/2}$, it was observed in^[14], strictly speaking, only experimentally⁶⁾.

We turn now to the case of high pressures, when the condition (22) is not satisfied ($p_0 > 1$ atm). In our experiments there was realized in this case a stationary plasmotron with one plasma region near the target surface, the dimensions of this region being several times larger than the diameter of the irradiated spot d (see Figs. 4b and 5b). The stationary dynamics of the plasma reduces in this case to a subsonic three-dimensional expansion of the target material from a hot and dense "core" with dimensions $\sim d$, located on the target surface and supplied with particles by evaporation. With increasing distance from the core, the plasma becomes cooler (as a result of recombination radiation and thermal conductivity), and the pressure in it approaches the external pressure p_0 ; the target-material plasma is then gradually mixed with the plasma of the surrounding gas.

In our experiments, the plasma region was symmetrical about the normal to the target surface, regardless of the angle of incidence of the laser beam (see Fig. 4b). This indicates that the temperature of the peripheral part of the plasma region is lower than the "ignition" temperature of the gas, and there is no slow "combustion" of the gas in the laser beam (see^[12]).

The authors thank A. M. Prokhorov for a discussion of the work.

¹⁾The electron losses to trapping with formation of negative ions can always be neglected at the considered vapor temperatures $T \sim T_{cr}$.

²⁾Even at $\sigma' = 10^{-14}$ cm² this condition calls for $\Delta < 200$ eV; we recall that the maximum first-ionization energy (for helium atoms) is 24.5 eV.

³⁾We note that the plasma-development regime described above was observed also in experiments on hydrogen breakdown^[13] by CO₂-laser radiation in the absence of a target; the radiation intensity in the focus was in that case $\sim 10^9$ w/cm². In the interpretation of the ionization wave, Offenberger and Burnet^[13] ignore the slow-combustion mechanism, and erroneously identify the stopping of the ionization front with the condition for the maintenance of the optical-detonation wave. This leads them to an incorrect conclusion that the experimental data on the dependence of I_{od} on p_0 do not agree with Raizer's theoretical prediction^[7]. In fact, as mentioned above, the threshold I_{od} increases with increasing pressure p_0 in agreement with Raizer's theory.

⁴⁾The increased power at the start of the pulse can also cause $I > I_{od}$ during this stage, and the stationary-plasmotron regime may be preceded by an optical-detonation regime. This picture of plasma development is shown in Fig. 5a.

⁵⁾It can be shown (this was done for metallic targets in^[2]) that $T > T_{boil}$ always. The conclusion drawn also in^[2] that the rule $T < T_{cr}$ for metals does not hold in general for nonmetallic targets; at the same time, under conditions when the plasmotron is stationary at a wavelength $\lambda = 10.6 \mu$, i.e., upper-bound estimate of the temperature T seems to be valid also for nonmetallic targets, inasmuch as we should have $I < I_{casc}$.

⁶⁾In^[14], we obtained for L/D the formula $L/d = [Mjv_1/(\gamma + 1)p_0]^{1/2}$, where the flux j is defined in (3). The dependence of the velocity v_1 on I was not established theoretically in these studies, and it was concluded on the basis of the experimental data for bismuth and aluminum that $v_1 \propto I^{1/2}$. It followed therefore that $L \propto I^{3/4}$, but this did not agree with the experimental data^[14], according to which $L \propto I^{1/2}$. The theoretical results obtained above eliminate this contradiction completely.

¹⁾A. I. Barchukov, F. V. Bunkin, V. I. Konov, and A. M. Prokhorov, *ZhETF Pis. Red.* 17, 413 (1973) [*JETP Lett.* 17, 294 (1973)].

²⁾V. A. Batanov, F. V. Bunkin, A. M. Prokhorov, and V. B. Fedorov, *Zh. Eksp. Teor. Fiz.* 63, 586 (1972) [*Sov. Phys.-JETP* 36, 311 (1973)].

³⁾S. I. Anisimov, Ya. A. Imas, G. S. Romanov, and Yu. V. Khodyko, *Deistvie izlucheniya bol'shoi moshchnosti na metally* (Effect of High-Power Radiation on Metals), Nauka (1970).

⁴⁾A. N. Pirri, R. Shlier, and D. Northam, *Appl. Phys. Lett.* 21, 79 (1972).

⁵⁾S. A. Ramsden and P. Savic, *Nature* 203, 1217 (1964).

⁶⁾Yu. P. Raizer, *Zh. Eksp. Teor. Fiz.* 48, 1508 (1965) [*Sov. Phys.-JETP* 21, 1009 (1965)].

⁷⁾Yu. P. Raizer, *ZhETF Pis. Red.* 7, 73 (1968) [*JETP Lett.* 7, 55 (1968)].

⁸⁾Ya. B. Zel'dovich and Yu. P. Raizer, *Fizika udarnykh voln i vysokotemperaturnykh gidrodinamicheskikh yavlenii* (Physics of Shock Waves and High-Temperature Hydrodynamic Phenomena), Nauka, 1966.

⁹⁾L. D. Landau and E. M. Lifshitz, *Mekhanika sploshnykh sred* (Fluid Mechanics), Gostekhizdat (1954) [Addison-Wesley, 1958].

¹⁰⁾F. V. Bunkin, V. I. Konov, A. M. Prokhorov, and V. B. Fedorov, *ZhETF Pis. Red.* 9, 609 (1969) [*JETP Lett.* 9, 371 (1969)].

¹¹⁾Yu. P. Raizer, *ZhETF Pis. Red.* 11, 195 (1970) [*JETP Lett.* 11, 120 (1970)], *Zh. Eksp. Teor. Fiz.* 58, 2127 (1970) [*Sov. Phys.-JETP* 31, 1148 (1970)].

¹²⁾Yu. P. Raizer, *Usp. Fiz. Nauk* 108, 429 (1972) [*Sov. Phys.-Usp.* 15, 688 (1972)].

¹³⁾A. A. Offenberger and N. H. Burnet, *J. Appl. Phys.* 43, 4977 (1972).

¹⁴⁾V. A. Batanov, F. V. Bunkin, A. M. Prokhorov, and V. B. Fedorov, *ZhETF Pis. Red.* 11, 113 (1970) [*JETP Lett.* 11, 69 (1970)], *Zh. Eksp. Teor. Fiz.* 63, 1240 (1972) [*Sov. Phys.-JETP* 36, 684 (1973)].

¹⁵⁾V. A. Batanov, F. V. Bunkin, A. M. Prokhorov, and V. B. Fedorov, *ZhETF Pis. Red.* 16, 378 (1972) [*JETP Lett.* 16, 266 (1972)].

Translated by J. G. Adashko
101